

## References

- 1 CARVER, K. A., and MINK, J. W.: 'Microstrip antenna technology', *IEEE Trans.*, 1981, AP-29, pp. 2-24
- 2 HALL, P. S., WOOD, C., and GARRETT, C.: 'Wide bandwidth microstrip antennas for circuit integration', *Electron. Lett.*, 1979, 15, pp. 458-460
- 3 CHEN, C. H., TULINTSEFF, A., and SORBELLO, R. M.: 'Broadband two-layer microstrip antenna'. Proceedings of 1984 international IEEE/APS symposium, Boston, pp. 251-255
- 4 GRIFFIN, J. M., and FORREST, J. R.: 'Broadband circular disc microstrip antenna', *Electron. Lett.*, 1982, 18, pp. 266-269
- 5 HARRINGTON, R. F.: 'Time-harmonic electromagnetic fields' (McGraw-Hill, New York, 1961), problem 7-35, p. 378
- 6 LEWIN, L.: 'Theory of waveguides' (Newnes-Butterworths, London, 1975), Section 5.4, pp. 152-158
- 7 PUES, H., and VAN DE CAPELLE, A.: 'Accurate transmission-line model for the rectangular microstrip antenna', *IEE Proc. H, Microwaves, Opt. & Antennas*, 1984, 131, pp. 334-340
- 8 MIRSHEKAR-SYAHKAL, D.: 'Analysis of uniform and tapered transmission lines for microwave integrated circuits'. Ph.D. thesis, University of London, 1979
- 9 PUES, H., and VAN DE CAPELLE, A.: 'Wideband impedance-matched microstrip resonator antennas'. Proceedings of 2nd ICAP, York, 1981, pp. 402-405
- 10 PUES, H., VAN KAUTEREN, A., VERCRUYSE, J., and VAN DE CAPELLE, A.: 'Broadband microstrip radar antenna element'. Proceedings of international conference on radar, Versailles, 1984

## DETECTION OF SEA-ICE FEATURES USING $K_a$ -BAND RADAR

Indexing term: Radar

Analysis of recorded radar data collected from a mixed field of Arctic ice shows that the  $K_a$ -band returns, more so than other frequencies, can be used to delineate targets that pose a threat or impediment to navigation. In particular, it is shown that the  $K_a$ -band returns highlight multiyear ice-floes, icebergs and first-year ice pressure ridges.

**Introduction:** Increased navigation in the Canadian Arctic and east coast offshore has placed a high demand on the development of sophisticated shipborne radar systems for detecting and classifying sea ice. To support research into the design of an improved radar system, the Canadian Department of Fisheries & Oceans and the Communications Research Laboratory of McMaster University, Canada, are conducting both theoretical and experimental programmes to develop a better understanding of the interaction between the transmitted signal from a surface-based radar and sea ice. Recent analysis of experimental data reveals the utility of  $K_a$ -band radar for the delineation of significant ice features. This letter presents some new results, and the authors believe that these are the first  $K_a$ -band surface-based radar results for sea ice.

Surface-based (shipborne) radars are the primary sensors used for navigating in ice. In an ice cover, icebergs and iceberg fragments represent a threat to the safety of a ship. Multiyear ice-floes, being much stronger than first-year ice, present an impediment to rapid transit. Normally, first-year ice poses little difficulty to an ice-breaking vessel, although large first-year pressure ridges can also be an impediment.

**Experimental programme:** An experimental radar programme was carried out in May 1983 in the Canadian Arctic to evaluate the utility of frequency and polarisation as possible radar discriminants in classifying sea ice. Radars were operated at S- (3 GHz), X- (9 GHz),  $K_u$ - (16 GHz) and  $K_a$ - (35 GHz) bands, with the three higher frequencies also providing dual-polarisation. Recordings were made with the antenna either scanning or fixed along a given radial. Several radial lines were chosen as standard lines, containing a variety of ice features that included first-year ice, multiyear ice, icebergs and iceberg fragments. The analysis in this letter will concentrate on data collected along the fixed radial lines.

The radar antennas were at a height of 30 m above the ice

surface, representing a grazing angle of between  $1.7^\circ$  and  $0.2^\circ$  over the 1-10 km range of interest.

To aid in target selection and ground truthing, the survey area was photographed with an aerial camera, yielding imagery of 1:20000 scale. The photographs were assembled into a photomosaic, covering approximately a 10 km radius around the radar.

To ensure the quality of the data, the radars were calibrated daily using externally injected signals. In addition, the transmitter output power, pulse repetition frequency, transmitter pulse length and wavelength losses were regularly measured.

Owing to low transmitter power and lossy waveguide, the  $K_a$ -band returns were considerably lower in amplitude than those from the other radars. Nevertheless, sufficient power was received from the targets of interest to allow useful comparison with the results obtained from the other radars.

**Results:** The recorded radar video was digitised and converted to received power using the measured calibration curves. To permit valid comparisons between radars, the radar equation was used to convert the received power to the normalised radar cross-section  $\sigma_0$ . The cross-section plots were scaled to match the appropriate section of the aerial photomosaic. Fig. 1 shows the ice surface corresponding to one of the stan-

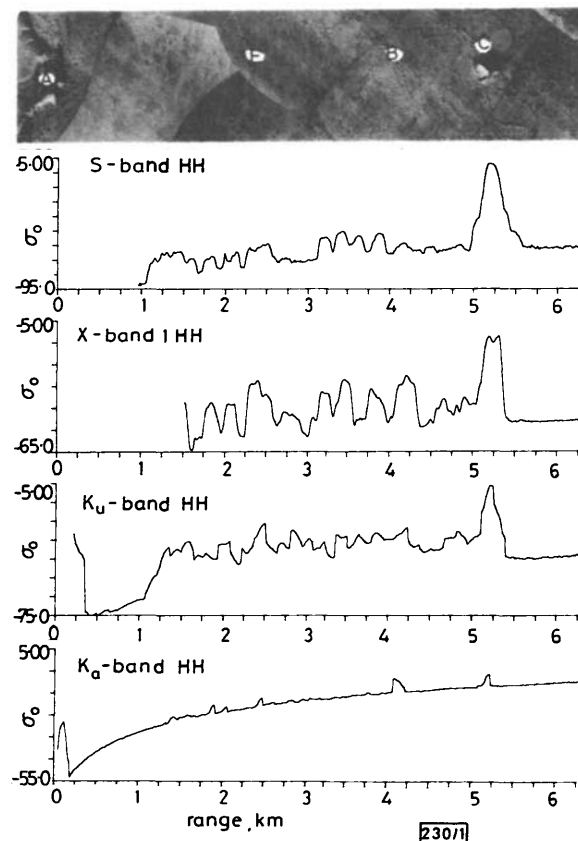


Fig. 1 Normalised radar cross-section against range for several radar frequencies along a fixed radial line

Line contains various ice features

A = radar site, B = multiyear ice-floe, C = iceberg, E = first-year pressure ridge

dard lines, with the cross-section plots for the S-, X-,  $K_u$  and  $K_a$ -band radars shown below. The radar systems were located on the shore at A, on the left-hand side of the image. The ice surface along the line is generally smooth, with some roughness in front of targets E and B. From a navigational perspective, the targets of interest are the first-year pressure ridge at location E, the multiyear ice-floe at B, and the iceberg at C.

The S-band return provides a relatively good indication of the surface roughness, and clearly detects the iceberg. However, it has not detected the multiyear flow at B, nor has it unambiguously detected the first-year pressure ridge at E. The X- and  $K_u$ -band plots are cluttered with returns from targets which are not navigationally significant. Both of these radars have detected the iceberg. While the X-band radar has detected the multiyear floe and the pressure ridge, it is not

possible to separate these returns from the other less significant background returns.

The  $K_a$ -band radar, despite its lower amplitude returns, clearly distinguishes the three targets of interest. The iceberg at C, the multiyear floe at B and the first-year pressure ridge at E are all clearly visible to the  $K_a$ -band radar. The source of the two smaller returns at 2 km range is not readily identifiable from the aerial photography. The property of the  $K_a$ -band radar to delineate significant targets, particularly multiyear ice, was demonstrated repeatedly in other standard lines. It is conjectured that this strong return from the multi-year floes results from a resonance effect between the relatively short  $K_a$ -band wavelength and the small drained (i.e. air-filled) brine pockets in the multiyear ice.

It is noteworthy that a similar highlighting of icebergs and multiyear ice is possible using crosspolarisation.<sup>1</sup> This effect, not limited to  $K_a$ -band radar, is felt to be due to depolarisation caused by the air inclusions present in both types of ice.

**Conclusion:** This letter has presented new results demonstrating the ability of a  $K_a$ -band radar to delineate sea ice features of significance to navigation. One of the reasons for this ability is suggested to be a resonance phenomenon occurring at the shorter  $K_a$ -band wavelength.

E. O. LEWIS

12th April 1985

Department of Fisheries & Oceans  
867 Lakeshore Road  
Burlington, Ontario, Canada L7R 4A6

S. HAYKIN  
B. W. CURRIE

Communications Research Laboratory  
McMaster University  
Hamilton, Ontario, Canada L8S 4K1

#### Reference

- HAYKIN, S., CURRIE, B. W., LEWIS, E. O., and NICKERSON, K. A.: 'Surface-based radar imaging of sea ice', *Proc. IEEE*, February 1985, special issue on radar, pp. 233-251

## WIDE-BANDWIDTH MODULATION OF THREE-CHANNEL BURIED-CRESCENT LASER DIODES

**Indexing terms:** Lasers and laser applications, Semiconductor lasers

The modulation bandwidth of three-channel buried-crescent (TCBC) lasers was improved by reducing the ohmic contact resistance by adding a quaternary contact layer for the P-contact of the device. The ohmic resistance was reduced to 6-9  $\Omega$ , with a capacitance of 1.5-3 pF and an inductance of 1.5-2 nH. The small-signal 3 dB modulation frequency is 7.2 GHz at  $2.5I_{th}$ , and is limited by the parasitic impedances of the device. Large-signal digital modulation of the laser was successfully achieved at 8 Gbit/s, which is the highest frequency for direct digital modulation yet reported.

**Introduction:** Wide-bandwidth three-channel buried-crescent (TCBC) lasers have been described in detail earlier.<sup>1,2</sup> These lasers have high modulation bandwidth, owing to the low parasitic capacitance that is associated with structures grown on semi-insulating substrates. A relatively high contact resistance in the previously described structure limited the 3 dB small-signal modulation bandwidth to 5-7 GHz.<sup>2</sup>

In the previous structure,<sup>1</sup> the P-contact was made on zinc-diffused InP. A lower contact resistance can be obtained by making the P-contact on a zinc-diffused quaternary layer. The modified grown layers and the final laser structure after processing are shown in Fig. 1. The first layer grown by liquid phase epitaxy is P-type quaternary (Fig. 1a), and this layer is exposed by selective etching on the right-hand side channel to

provide a window opening for the following zinc diffusion (see Fig. 1b). By introducing these modifications, the ohmic resistance was reduced by 6-9  $\Omega$ , and the parasitic capacitance and

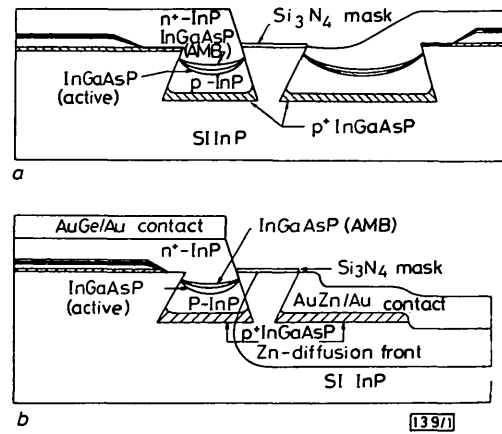


Fig. 1

- Schematic cross-section of LPE grown layers
- Schematic cross-section of laser diode

inductance for laser chips mounted on copper studs were measured to be 1.5-3 pF and 1.5-2 nH, respectively.

**Device performance:** The CW characteristics of these lasers are similar to those reported earlier,<sup>2</sup> with threshold currents of 20 mA and peak CW power of 8 mW/facet at 15°C. Measured small-signal frequency response curves are shown in Fig. 2.

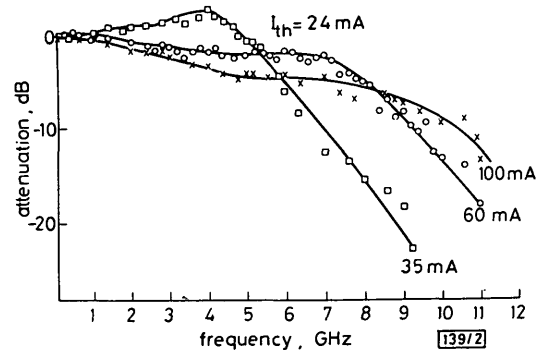


Fig. 2 Small-signal frequency response of laser diode

The widest bandwidth was obtained at 60 mA ( $2.5I_{th}$ ). The response drops to 3 dB below its low-frequency value at 7.2 GHz. The dependence of the 3 dB bandwidth on the output light power for a different device from the same batch is shown in Fig. 3. The slope of the curve is 4.4 GHz/mW<sup>1/2</sup>, which corresponds to a 10 GHz bandwidth at roughly 5 mW output power. The laser response, however, is still limited by the parasitic impedances of the device, which cause the sharp decrease in the bandwidth at power levels above 3 mW, as shown in Fig. 3.

The large-signal digital modulation response was measured using a pseudorandom nonreturn-to-zero word generator at

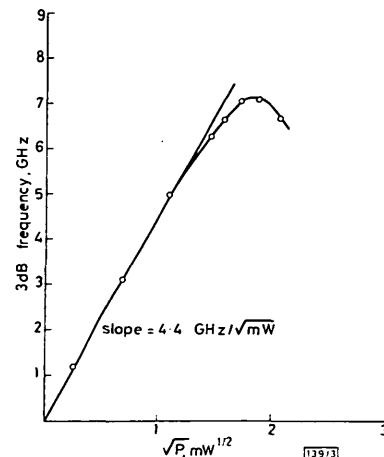


Fig. 3 Dependence of 3 dB small-signal modulation bandwidth on output light power